Supporting Information

Wang et al. 10.1073/pnas.0902281106

SI Text

Detailed Experimental Procedures. ***Damaged DNA probes.*** Unmodified, tetramethylrhodamine (TMR) labeled, and 6-carboxylfluorescein (FAM) labeled single stranded oligodeoxynucleotides were synthesized and purified by Integrated DNA Technologies. The sequences and their modification are listed in Table S1. A BPDE-16-mer that contained a single BPDE-N^2 deoxyguanosine (dG) adduct was synthesized by the direct reaction of (±)anti-BPDE and an oligo with the sequence 5′-CCCATTA*TGC*ATA-ACC-3′ as described previously (1). To carry out CE-LIFP and CE-FRET binding studies, a number of damaged probes (listed in Table S2) were constructed from these oligonucleotides. Construction was performed through ligation of unmodified or modified 16mer (oligo 3) with 5 other oligonucleotides in equimolar ratio (listed in Table S2). The TMR-GAP-ds90mer was an exception, because it was prepared by ligation of only 5 oligonucleotides, i.e., without including a 16mer (oligo 3, Table S2). The ligation was carried out according to the protocol described previously (1) with minor modifications. The ligated products were purified using 16.0% polyacrylamide gel electrophoresis. The concentrations of the damaged DNA probes were estimated using UV absorbance at 260 nm.

CE-FRET. The CE-FRET instrument was modified from a laboratory-constructed CE-LIFP system described previously (2, 3). An argon ion laser with an excitation wavelength of 488 nm (model 2214-65, Uniphase) was used to excite 6-carboxylfluorescein (FAM) in the FRET DNA probes. Instead of a polarized beam splitter used in the CE-LIFP system, a dichroic mirror (Melles Griot) was used in the CE-FRET system to transmit fluorescent light of 580 nm to one PMT and to reflect the fluorescence at 515 nm to the second PMT. Bandpass interference filters of 515 nm and 580 nm with a FWHM of 10 nm (Melles Griot) were placed before the corresponding PMTs, and the fluorescence intensities detected by the 2 PMTs provided FRET information. The output from the PMT and the CE high voltage were controlled using application software written in Labview (National Instruments) and a PCI data acquisition board housed inside a Power Macintosh computer.

Fluorescence lifetime measurements. Time-resolved fluorescence intensity decay data were collected using a time-correlated, single-photon counting instrument, described previously (4). Excitation was with 2 picosecond pulses (full-width at half-maximum) of vertically polarized laser light, at a repetition rate of 76.8 MHz using a Mira-OPO (Coherent Inc.) pumped by a Mira 900 Ti:Sapphire laser (Coherent Inc.). The emission path, at 90° to the excitation, passed through a polarizer oriented at 54.7° from vertical [the magic angle condition (5)] to eliminate intensity artifacts due to molecular rotation. The emission wavelength was selected by using either a monochromator with a 20-nm band-pass or 25-nm band-pass filters. Intensity decay curves and corresponding instrument response functions were collected with a timing calibration of 22 picoseconds per channel into 2000 channels. The decay curves were collected to 40,000 peak counts. The response function for each decay curve was measured using a light-scattering solution of dilute colloidal silica and collected to 100,000 peak counts. Datasets were analyzed by a standard reconvolution procedure (6), using nonlinear regression (7), and the intensity decay, $I(t)$, was fit as a sum of exponentials:

$$I(t) = \sum_{i=1}^{n} \alpha_i \, e^{-t/\tau_i} \qquad \textbf{[S1]}$$

where the preexponential factor α_i is the amplitude of each component and τ_i is the associated fluorescence lifetime. The recovered decay parameters were then used to calculate the intensity-weighted lifetime:

$$< \tau > \; = \sum_{i=1}^{n} \alpha_i \, \tau_i^2 / \sum_{i=1}^{n} \alpha_i \, \tau_i \, . \qquad \textbf{[S2]}$$

Estimation of binding constants. For the binding of UvrA to the damage DNA probe, the binding constants can be calculated according to Eq. **S3**:

$$K = \frac{[UvrA_2 \cdot DNA]}{[UvrA_2][DNA]} \qquad \textbf{[S3]}$$

In Eq. **S3**, the ratio of [$UvrA_2$·DNA] to [DNA] can be directly measured from CE-LIF analysis, and the unbound (free) concentration of UvrA dimer ([$UvrA_2$] can be derived from the concentrations of total UvrA, total DNA probe, and bound DNA probe. The total concentrations of UvrA and the DNA probe are known, and the bound concentration of the DNA probe can be estimated from CE-LIFP analysis.

For the binding constants of $UvrA_2B$ (or $UvrA_2B_2$) to the DNA probe, the estimation was obtained as below:

$$K = \frac{[UvrA_2 B \cdot DNA]}{[UvrA_2 B][DNA]} \qquad \textbf{[S4]}$$

where the concentration of $UvrA_2B$ was estimated by assuming that all $UvrA_2$ can form $UvrA_2B$ in the presence of excess UvrB. The free concentration of $UvrA_2B$ was estimated by subtracting the UvrB bound to DNA, which was measurable from CE-LIF analysis.

CE-LIFP analysis of the mixture of UvrA, UvrB, and TMR-BP-ds90mer in the presence of ATP or ATPγS. Recent work suggests that ATP binding by UvrB is sufficient for formation of the $UvrA_2B$ complex (8) and preincision UvrB(UvrA)·DNA complex (9), but hydrolysis is required for the formation of the UvrB·DNA preincision complex (9). Therefore, if nonhydrolysable ATPγS is used in place of normal ATP, only $UvrA_2B$·TMR-BP-ds90mer should be formed and the formation of UvrB·TMR-BP-ds90mer should be inhibited. In the presence of ATPγS, indeed only one UvrB-containing DNA complex formed, which had a large polarization value (P = 0.353) and shorter migration time (Fig. S1, lower trace). Furthermore, in the presence of ATPγS, the peak of $UvrA_2B$·TMR-BP-ds90mer was approximately twice as large as the corresponding product generated in the presence of ATP (Fig. S1, upper trace), and the UvrB·TMR-BP-ds90mer (second UvrB-DNA complex) disappeared. [The peak with the same migration time is much smaller and has a moderate polarization value (P = 0.279)]. These results suggest that the UvrB-containing DNA complex with faster migration was the heterotetrameric complex, $UvrA_2B$·TMR-BP-ds90mer, and the other slower migrating complex was UvrB·TMR-BP-ds90mer. In our free zone CE approach, the faster migration of $UvrA_2B$·TMR-BP-ds90mer (Fig. 1*A*) is also consistent with its larger negative mass-to-charge ratio.

AFM analysis revealed the presence of 2 UvrB proteins in the UvrB-containing DNA complexes (10), thus it is possible to form 2 more UvrB-containing DNA complexes, $UvrA_2B_2$·TMR-BP-ds90mer and $UvrB_2$·TMR-BP-ds90mer. In such complexes, one

UvrB binds the DNA tightly but the second UvrB binds the DNA loosely (11). In our CE-LIFP analysis, only 2 UvrB-DNA complexes were observed. The same 2 peaks were observed when we substituted *Bacillus caldotenax* UvrBΔ4 for the wild-type *E. coli* protein. Since the mutant UvrBΔ4 has lost the ability to form a UvrB dimer (12, 13), we excluded the possibility that the 2 observed complexes were due to $UvrA_2B_2$·TMR-BP-ds90mer and $UvrB_2$·TMR-BP-ds90mer. No observation of $UvrA_2B_2$·DNA and $UvrB_2$·DNA complexes is probably due to the dissociation of the second UvrB in these 2 complexes during CE-LIFP analysis. This is consistent with a previous report by Moolenaar et al. (11) They observed that the second loosely bound UvrB in the UvrB-DNA complexes often dissociated during gel electrophoresis.

Time-resolved fluorescence lifetime analysis supports the conformational change of DNA in UvrB-DNA complexes. To investigate the conformational changes induced at the site of the adduct, we studied the fluorescence lifetime of the damage probes and their protein complexes using time-resolved fluorescence lifetime analysis (Table S4). For TMR-ds90mer and TMR-BP-ds90mer, the average lifetimes were almost identical ($\tau = 2.03$ ns vs. $\tau = 2.04$ ns), indicating no measurable probe perturbations induced by the BPDE-dG adduct. In other words, based on the optimal fitting of fluorescence intensity decay curves, there is no significant change in the rotation modes caused by the BPDE-dG adduct. In addition, incubation of TMR-BP-ds90mer with *E. coli* UvrA did not induce a change in fluorescence lifetime ($\tau = 2.06$ ns vs. $\tau = 2.04$ ns), indicating that within the limitations of the method, the binding to UvrA did not reveal a conformational change of the damage probe. On the other hand, the binding of TMR-BP-ds90mer to *E. coli* UvrAB did appear to cause a conformational change of the TMR-BP-ds90mer, because the average lifetime increased from 2.044 ns to 2.212 ns after the binding. The optimal fitting of the intensity decay data suggests that close contact of the protein(s) to the TMR in the damage probe results in significant restriction of the local rotation of TMR and this restriction of the local rotation of TMR leads to increased polarization of the fluorescence. This observation supports our hypothesis that the large polarization values are linked to DNA wrapping of UvrB because it implies that UvrB makes intimate contact with both the site of damage (BPDE-adduct) and the TMR label situated 45 bp from the damage site.

DNA wrapping of UvrB stabilizes the UvrB-DNA complexes. With the wrapping of DNA around the protein and the multipoint close contact, a more stable binding would be expected. It is indeed interesting to note that a gapped DNA duplex, analogous to that formed after removal of 12–14 nucleotides from double-stranded DNA during the *E. coli* NER process, not only forms a stable complex with UvrB (loaded by UvrA), but also wraps around UvrB ($P = 0.366 \pm 0.007$) (see Fig. S5). The binding constant for the UvrB-gapped DNA complex is approximately $3.7 \times 10^8\ M^{-1}$. In contrast, UvrB has low affinity for normal DNA (single-stranded or double-stranded) regardless of the presence or absence of UvrA. In our experiments, we show that in the presence of UvrA, UvrB has moderate affinity for end-labeled dsDNA ($K_a \approx 1.1 \times 10^7\ M^{-1}$). Similarly, Hsu et al. have shown a weak affinity of UvrB for single stranded DNA whether or not DNA is damaged (14). Thus, the affinity of UvrB to ssDNA and dsDNA is much lower (>30-fold) than that of UvrB binding to the gapped DNA ($K_a \approx 3.7 \times 10^8\ M^{-1}$). These results suggest that DNA wrapping of UvrB greatly contributes to the formation of a stable complex with gapped DNA, which is a substrate of the Uvr ABC system (8). This suggestion is consistent with previous work showing no detectable turnover of UvrB-UvrC complex in vitro in the absence of *E. coli* Pol1 and UvrD protein (15–17).

1. Carnelley T, et al. (2001) Synthesis, characterization, and applications of a fluorescent probe of DNA damage. *Chem Res Toxicol* 14:1513–1522.
2. Wan Q-H, Le XC (1999) Fluorescence polarization studies of affinity interactions in capillary electrophoresis. *Anal Chem* 71:4183–4189.
3. Wan Q-H, Le XC (2000) Studies of protein-DNA interactions by capillary electrophoresis laser-induced fluorescence polarization. *Anal Chem* 72:5583–5589.
4. Rachofsky EL, Osman R, Ross JB (2001) Probing structure and dynamics of DNA with 2-aminopurine: Effects of local environment on fluorescence. *Biochemistry* 40:946–56.
5. Lakowicz JR (2006) *Principles of Fluorescence Spectroscopy* (Springer, New York), 3rd Ed.
6. Grinvald A, Steinberg IZ (1974) On the analysis of fluorescence decay kinetics by the method of least-squares. *Anal Biochem* 59:583–98.
7. Bevington PR (1969) *Data Reduction and Error Analysis for the Physical Sciences* (McGraw-Hill, New York).
8. Della Vecchia MJ, et al. (2004) Analyzing the handoff of DNA from UvrA to UvrB utilizing DNA-protein photoaffinity labeling. *J Biol Chem* 279:45245–45256.
9. Moolenaar GF, et al. (2000) The role of ATP binding and hydrolysis by UvrB during nucleotide excision repair. *J Biol Chem* 275:8044–8050.
10. Verhoeven EE, Wyman C, Moolenaar GF, Goosen N (2002) The presence of two UvrB subunits in the UvrAB complex ensures damage detection in both DNA strands. *EMBO J* 21:4196–4205.
11. Moolenaar GF, Schut M, Goosen N (2005) Binding of the UvrB dimer to non-damaged and damaged DNA: residues Y92 and Y93 influence the stability of both subunits. *DNA Repair* 4:699–713.
12. Zou Y, et al. (2004) DNA damage recognition of mutated forms of UvrB proteins in nucleotide excision repair. *Biochemistry* 43:4196–4205.
13. Wang H, et al. (2006) UvrB domain 4, an autoinhibitory gate for regulation of DNA binding and ATPase activity. *J Biol Chem* 281:15227–15237.
14. Hsu DS, Kim ST, Sun Q, Sancar A (1995) The structure and function of UvrB protein. *J Biol Chem* 270:8319–8327.
15. Caron PR, Kushner SR, Grossman L (1985) Involvement of helicase II (*uvrD* gene product) and DNA polymerase I in excision mediated by the UvrABC protein complex. *Proc Natl Acad Sci USA*, 82:4925–4929.
16. Husain I, Van Houten B, Thomas DC, Abdel-Monem M, Sancar A (1985) Effect of DNA polymerase I and DNA helicase II on the turnover rate of UvrABC excision nuclease. *Proc Natl Acad Sci USA*, 82:6774–6778.
17. Friedberg EC, et al. (2006) *DNA Repair and Mutagenesis* (ASM Press, Washington, DC), 2nd Ed, pp 249–250.

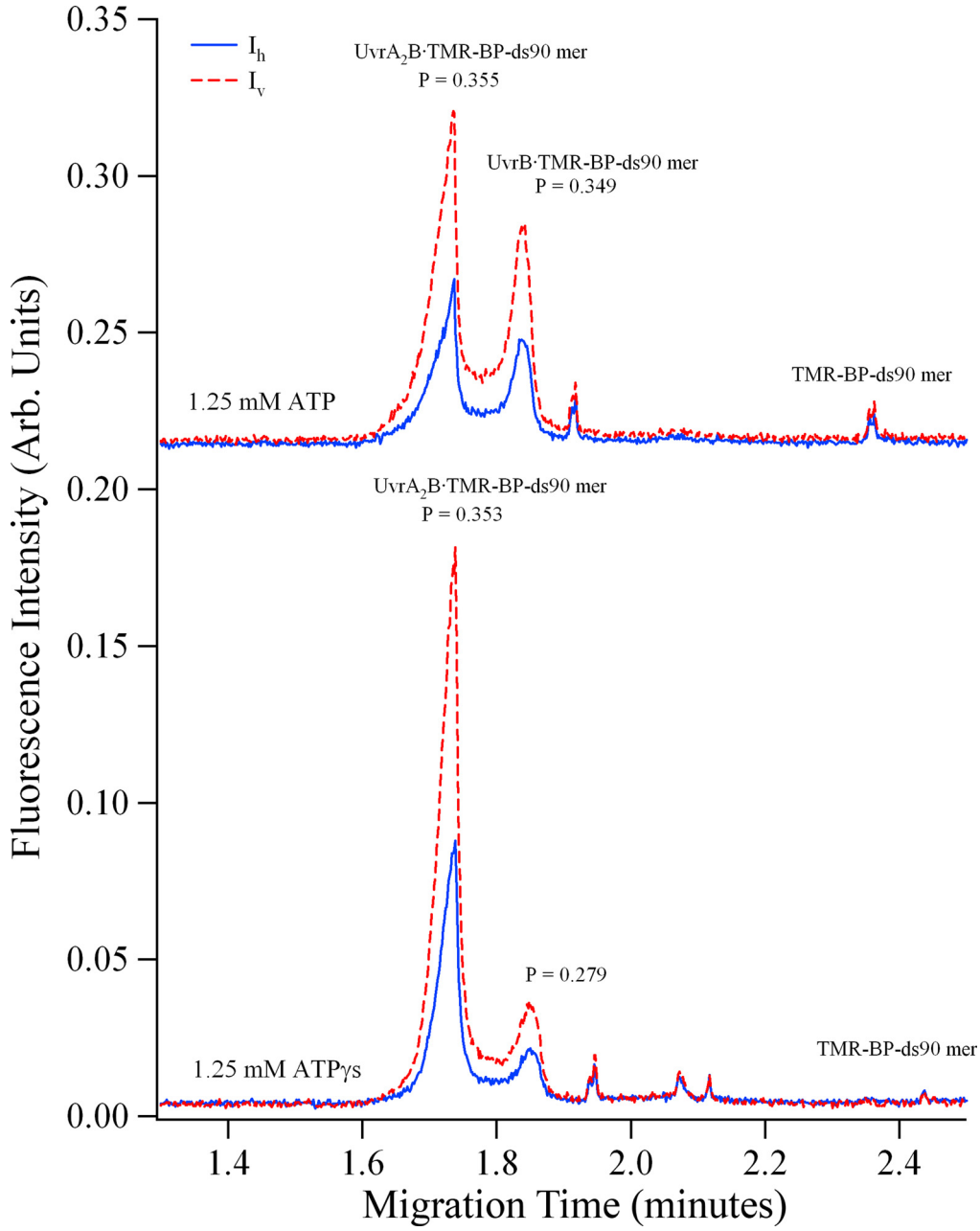

Fig. S1. CE-LIFP analysis of the mixture of UvrA, UvrB, and TMR-BP-ds90 mer in the presence of ATP or ATPγS, showing the identification of two UvrB-containing DNA complexes, $UvrA_2B$·TMR-BP-ds90 mer and UvrB·TMR-BP-ds90 mer. The peak at ~1.85 min in the bottom trace is unidentified. The concentrations of DNA substrate and proteins used in these experiments were 5 nM TMR-BP-ds90 mer, 40 nM UvrA, and 40 nM UvrB.

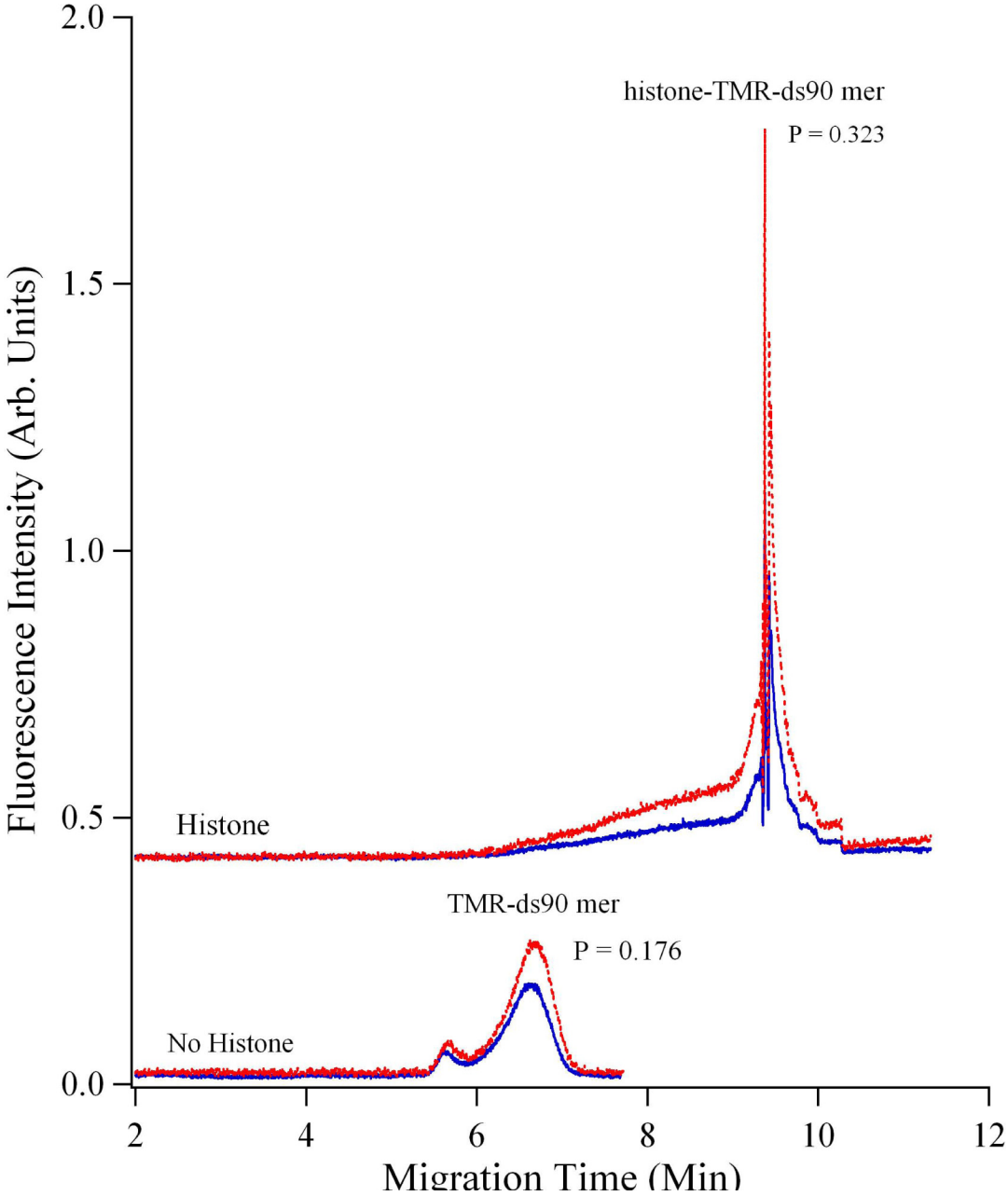

Fig. S2. CE-LIFP analysis of interaction of TMR-ds90mer with a bovine histone protein preparation (primarily histone H1), showing large polarization.

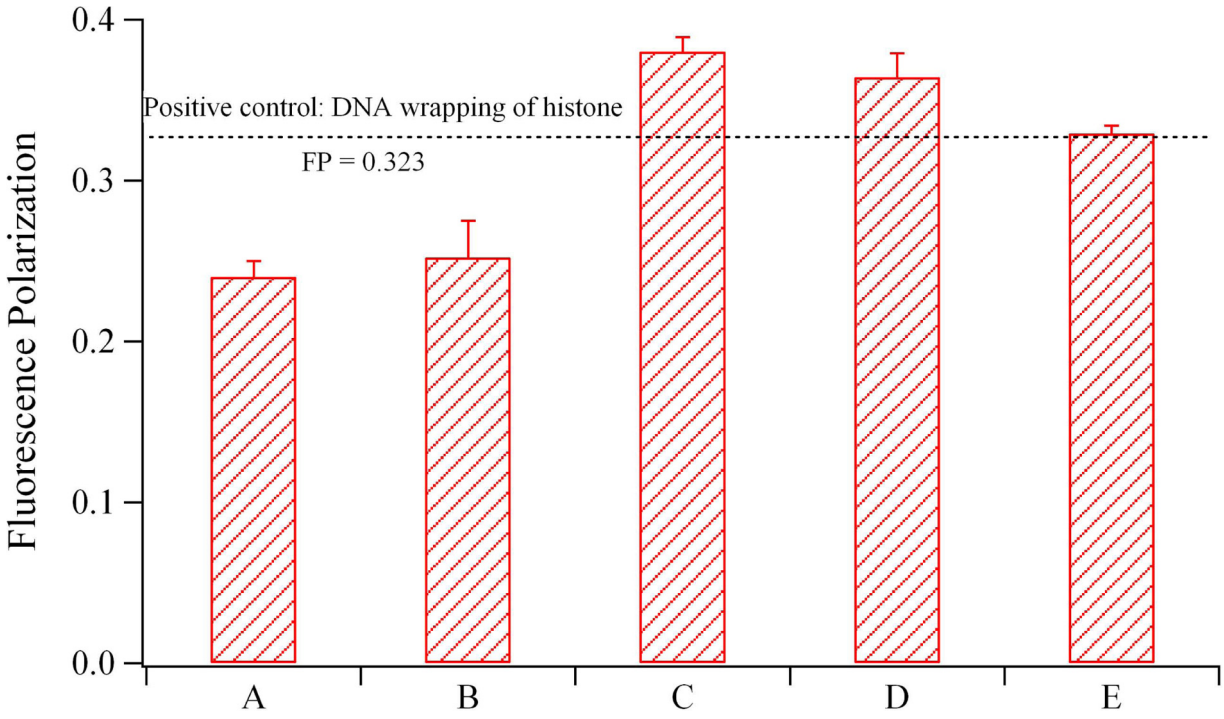

Fig. S3. Fluorescence polarization of mutant UvrB-DNA complexes. The fluorescence polarization values of TMR-BP-ds90mer (A), the complex of *E. coli* UvrA and TMR-BP-ds90mer (B), and the complexes of $UvrA_2B$·TMR-BP-ds90 mer with *E. coli* UvrA and *B. caldotenax* wtUvrB (C), or *B. caldotenax* UvrBΔ4 (D), or *B. caldotenax* UvrBY96A (E).

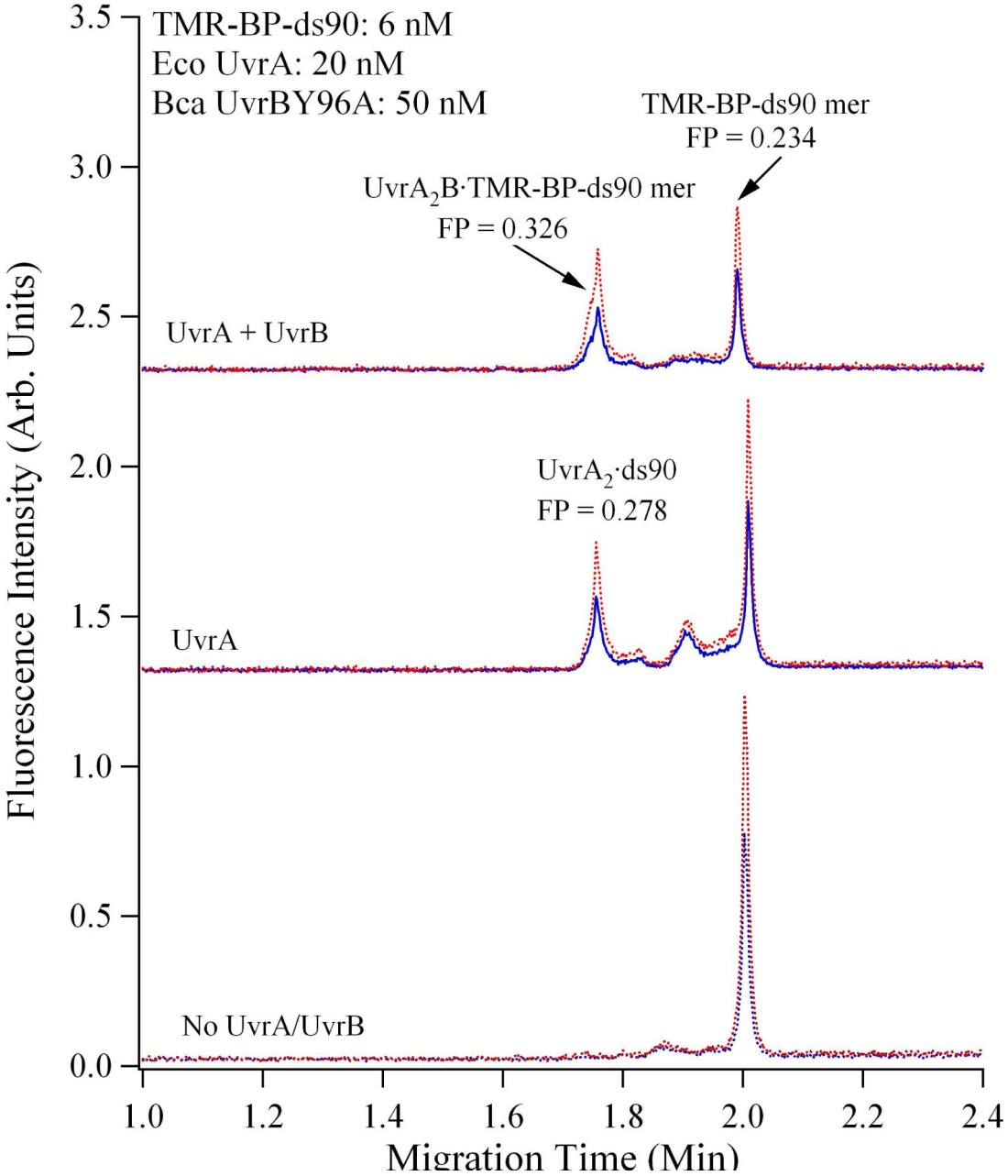

Fig. S4. CE-LIFP analysis of the binding of mutant UvrBY96A to the TMR-BP-ds90 mer, showing the formation of UvrAUvrB-DNA complex and the absence of preincision UvrB-DNA complex. The reaction and CE-LIFP analysis conditions are the same as those described in Fig. 1.

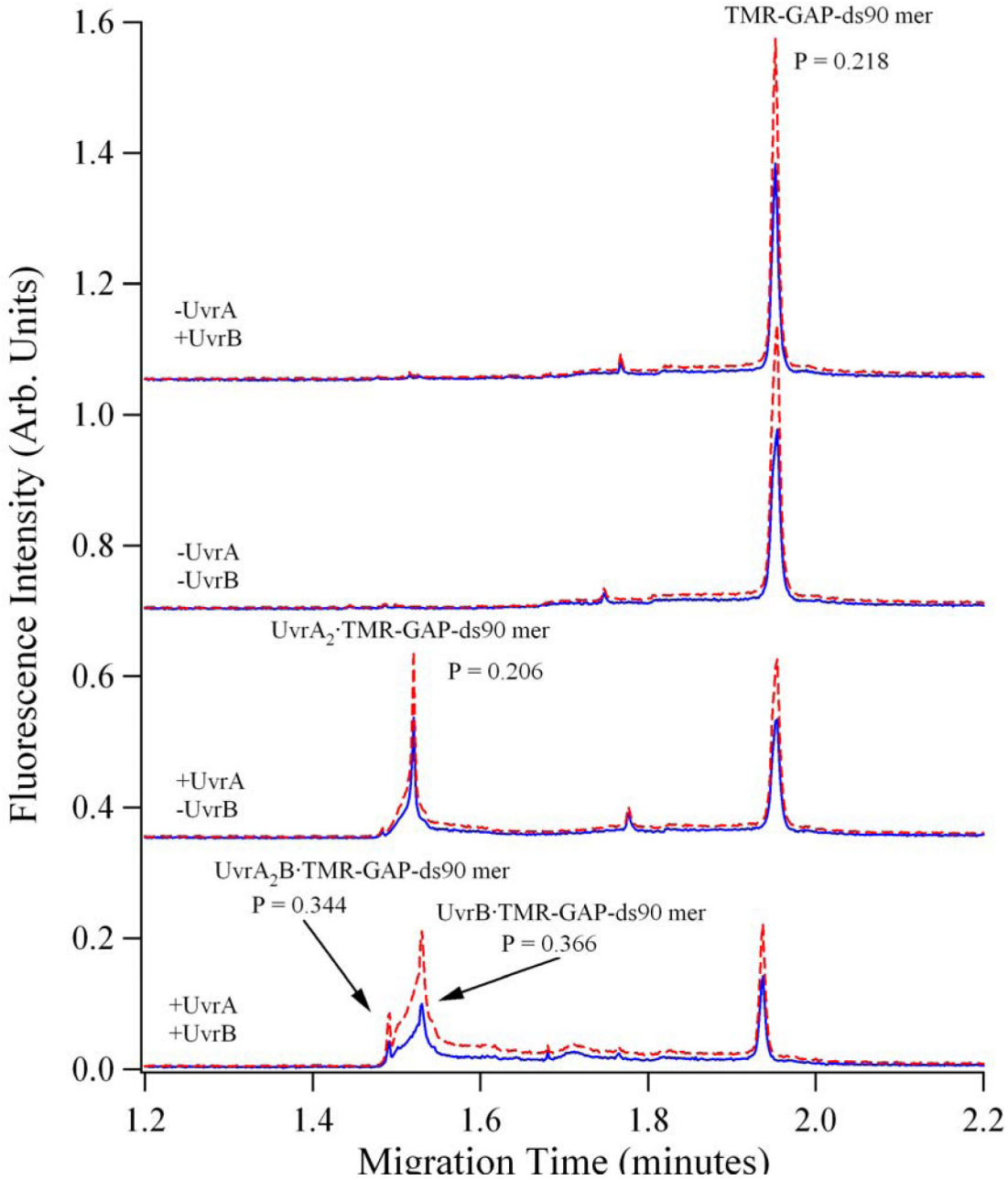

Fig. S5*A*. CE-LIFP analysis of TMR-gap-ds90 mer and its binding to *E.coli* UvrAB. The reaction and CE-LIFP analysis conditions are the same as those described in Fig. 1.

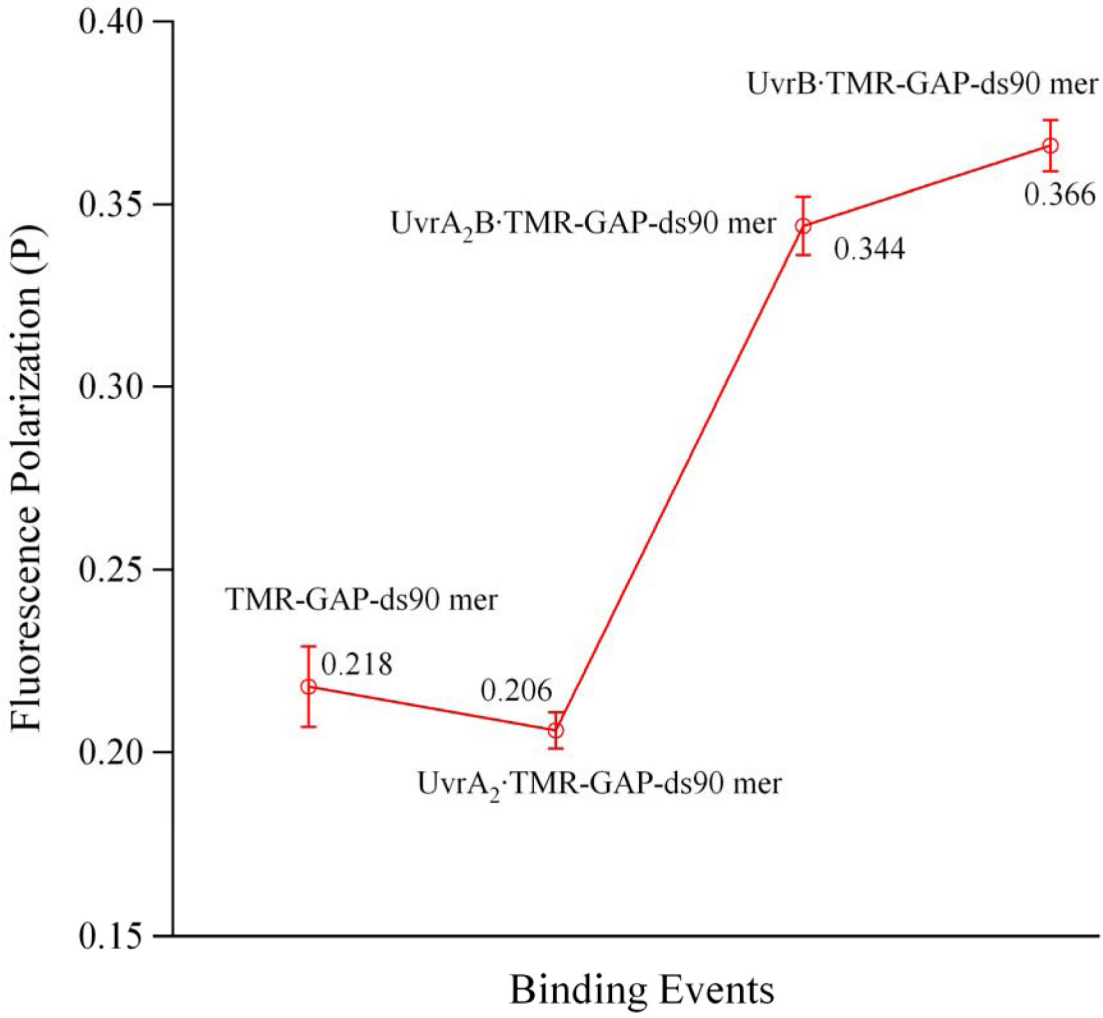

Fig. S5*B*. The course of fluorescence polarization of a gapped DNA substrate versus binding events, showing DNA wrapping after UvrB binding to the probe.

Other Supporting Information Files

Table S1 (PDF)
Table S2 (PDF)
Table S3 (PDF)
Table S4 (PDF)